The relation of cosmic environment and morphology with the star formation and stellar populations of AGN and non-AGN galaxies

Mountrichas, G.; Yang, G.; Buat, V.; Darvish, B.; Boquien, M.; Ni, Q.; Burgarella, D.; Ciesla, L.

Published in:
Astronomy and astrophysics

DOI:
10.1051/0004-6361/202346706

A&A 675, A137 (2023)
https://doi.org/10.1051/0004-6361/202346706

Astronomy & Astrophysics

The relation of cosmic environment and morphology with the star formation and stellar populations of AGN and non-AGN galaxies

G. Mountrichas[1], G. Yang[2,3], V. Buat[4,5], B. Darvish[6], M. Boquien[7], Q. Ni[8], D. Burgarella[4], and L. Ciesla[4]

[1] Instituto de Fisica de Cantabria (CSIC-Universidad de Cantabria), Avenida de los Castros, 39005 Santander, Spain
e-mail: gmountrichas@gmail.com
[2] Kapteyn Astronomical Institute, University of Groningen, PO Box 800, 9700 AV Groningen, The Netherlands
[3] SRON Netherlands Institute for Space Research, Postbus 800, 9700 AV Groningen, The Netherlands
[4] Aix Marseille Univ, CNRS, CNES, LAM, Marseille, France
[5] Institut Universitaire de France (IUF), 75005 Paris, France
[6] University of California, 900 University Avenue, Riverside, CA 92521, USA
[7] Centro de Astronomía (CITEVA), Universidad de Antofagasta, Avenida Angamos 601, Antofagasta, Chile
[8] Max-Planck-Institut für extraterrestrische Physik (MPE), Gießenbachstraße 1, 85748 Garching bei München, Germany

Received 19 April 2023 / Accepted 5 June 2023

ABSTRACT

In this work, we study the relation of the cosmic environment and morphology with the star formation and stellar population of galaxies. Most importantly, we examine if this relation differs for systems with active and non-active supermassive black holes. For that purpose, we used 551 X-ray detected active galactic nuclei (AGNs) and 16 917 non-AGN galaxies in the COSMOS-Legacy survey for which surface-density field measurements are available. The sources lie at a redshift of $0.3 < z < 1.2$, probe X-ray luminosities of $42 < \log[L_{\rm X,2-10\,keV}(\rm erg\,s^{-1})] < 44$, and have stellar masses of $10.5 < \log[M_*(M_\odot)] < 11.5$. Our results show that isolated AGNs (field) have lower star formation rates (SFRs) compared to non-AGNs at all $L_{\rm X}$ spanned by our sample. However, in denser environments (filaments and clusters), moderate $L_{\rm X}$ AGN ($\log[L_{\rm X,2-10\,keV}(\rm erg\,s^{-1})] > 43$) and non-AGN galaxies have similar SFRs. We also examined the stellar populations and the morphology of the sources in different cosmic fields. For the same morphological type, we find that non-AGN galaxies tend to have older stellar populations and are less likely to have undergone a recent burst in denser environments compared to their field counterparts. The differences in the stellar populations concerning density field are mainly driven by quiescent systems. Moreover, low $L_{\rm X}$ AGNs present negligible variations of their stellar populations in all cosmic environments, whereas moderate $L_{\rm X}$ AGNs have, on average, younger stellar populations and are more likely to have undergone a recent burst in high-density fields. Finally, in the case of non-AGN galaxies, the fraction of bulge-dominated (BD) systems increases with the density field, while BD AGNs are scarce in denser environments. Our results are consistent with a scenario in which a common mechanism, such as mergers, triggers both the star-formation and the AGN activity.

Key words. galaxies: active – galaxies: clusters: general – X-rays: galaxies – X-rays: general – galaxies: evolution

1. Introduction

It is widely accepted that galaxies and the supermassive black hole (SMBH) in their centres co-evolve. This symbiosis has been demonstrated in a variety of ways. For instance, tight correlations have been found between the black hole mass and various galaxy properties (e.g., bulge or stellar mass, stellar velocity dispersion; Magorrian et al. 1998; Ferrarese & Merritt 2000; Tremaine et al. 2002; Kormendy & Ho 2013). Moreover, both the SMBH activity and star formation activity peak at similar cosmic times ($z \sim 2$; e.g., Boyle et al. 2000; Sobral et al. 2013). In addition, both the black hole and galaxy growth are fed by cold gas.

A popular method to examine the co-evolution of galaxies and SMBHs is to study the relation between the star formation rate (SFR) of the galaxy and the accreting power of the SMBH in their centre. For the latter, X-ray luminosity, $L_{\rm X}$, is used as a proxy in galaxies that host active SMBHs. These galaxies are known as active galactic nuclei (AGNs). Although the investigation of this relation has been the topic of many studies (e.g., Lutz et al. 2010; Page et al. 2012; Lanzuisi et al. 2017), more information can be gained regarding the effect of the AGN feedback on the host galaxy by comparing the SFRs of AGNs with those of non-AGN systems with a similar stellar mass, M_*, and redshift (e.g., Rosario et al. 2013; Mullaney et al. 2015; Masoura et al. 2018, 2021; Bernhard et al. 2019; Florez et al. 2020; Koutoulidis et al. 2022; Pouliasis et al. 2022). Recent studies that applied this method have found that for galaxies with $10.5 < \log[M_*(M_\odot)] < 11.5$, the SFRs of low-to-moderate $L_{\rm X}$ ($42 < \log[L_{\rm X,2-10\,keV}(\rm erg\,s^{-1})] < 44$) AGNs tend to be either lower or at most equal to the SFRs of non-AGN star forming galaxies, while an enhancement of ∼30% was found for the SFRs of galaxies that host higher $L_{\rm X}$ AGNs compared to non-AGN systems. Nevertheless, in both lower-mass and more massive galaxies, the SFRs of AGNs were similar to that of non-AGN systems (Mountrichas et al. 2021, 2022a,c). These results have also been supported by studying the stellar populations of low-to-moderate $L_{\rm X}$ AGNs compared to non-AGN systems (Mountrichas et al. 2022b).

A limitation of the above works is that they do not take into account the cosmic environment of the two populations (i.e., AGN and non-AGN systems). A significant number of studies, though, have investigated if and how the cosmic web affects the star formation of galaxies (non-AGN) both in the local Universe

and at high redshifts (e.g., Pandey & Sarkar 2020; Das et al. 2021; Brambila et al. 2023; Song et al. 2023). At low redshifts ($z < 1$), most studies suggest that quiescent (Q) galaxies preferentially live in dense environments, such as groups and clusters, whereas star-forming galaxies are more commonly found in the field (e.g., Lin et al. 2014; Erfanianfar et al. 2016). A plausible scenario to interpret these results is that cold gas is removed from satellite galaxies due to their interaction with the warm intracluster medium. At high redshifts, though, this picture seems to be either reversed (e.g., Elbaz et al. 2007; Santos et al. 2014) or there is no difference that has been found in the SFRs of galaxies that live in different density fields (e.g., Scoville et al. 2013; Cooke et al. 2023). Furthermore, a number of studies have shown that one of the galaxy properties that is most influenced by the cosmic environment is galaxy morphology (e.g., Dressler 1980; Fasano et al. 2015). Nevertheless, these studies do not take into account the activity of the SMBH. In other words, they do not differentiate between AGN and non-AGN galaxies.

In this work, we compare the SFRs and star formation histories (SFHs) of AGN and non-AGN systems for different cosmic environments (i.e., field, filaments, clusters) and morphologies, namely, bulge dominated (BD) and non-bulge dominated (non-BD). Our goal is to examine the effect of AGN feedback on the host's star formation in different density fields and to compare the role of the cosmic web and morphology on the stellar population of AGN and non-AGN galaxies. For that purpose, we used sources detected in the COSMOS field that lie at $z \sim 1$. We computed M_* by applying spectral energy distribution (SED) fitting using the CIGALE code, probing a range of $10.5 < \log[M_*(M_\odot)] < 11.5$. In this work, we first compare the SFRs of galaxies that host AGNs with their non-AGN counterparts as a function of the cosmic environment. Then, we compare the effect of the density field and morphology on the stellar populations of AGN and non-AGN galaxies. Finally, we discuss our results and describe our main conclusions. Throughout this work, we assume a flat ΛCDM cosmology with $H_0 = 70.4\,\mathrm{km\,s^{-1}\,Mpc^{-1}}$ and $\Omega_\mathrm{M} = 0.272$ (Komatsu et al. 2011).

2. Data

2.1. The X-ray dataset

In this study, we used sources that lie within the COSMOS field (Scoville et al. 2007). The X-ray AGNs have been observed by the COSMOS-Legacy survey (Civano et al. 2016). This is a 4.6 Ms *Chandra* programme that covers 2.2 deg^2 of the COSMOS region. The central area has been observed with an exposure time of ≈160 ks, while the remaining area has an exposure time of ≈80 ks. The limiting depths are 2.2×10^{-16}, 1.5×10^{-15}, and 8.9×10^{-16} erg cm^{-2} s^{-1} in the soft (0.5–2 keV), hard (2–10 keV), and full (0.5–10 keV) bands, respectively. The X-ray catalogue includes 4016 sources. Marchesi et al. (2016) matched the X-ray sources with optical and infrared counterparts using the likelihood ratio technique (Sutherland & Saunders 1992). Of the sources, 97% have an optical and IR counterpart and a photometric redshift (photo-z), and ≈54% have spectroscopic redshift (spec-z). Photo-z have been derived from high-quality ultraviolet-to-infrared data (up to 32 bands; Laigle et al. 2016). Hardness ratios ($HR = \frac{H-S}{H+S}$, where H and S are the net counts of the sources in the hard and soft band, respectively) were estimated for all X-ray sources using the Bayesian estimation of hardness ratios method (BEHR; Park et al. 2006). The intrinsic column density, N_H, for each source was then calculated using its redshift and assuming an X-ray spectral power law with slope $\Gamma = 1.8$. This information is available in the catalogue presented in Marchesi et al. (2016). In this work, we used sources within the UltraVISTA region (1.38 deg^2 McCracken et al. 2012) of the COSMOS field. There are 1718 X-ray sources within this region with $\log[L_{\mathrm{X,2-10\,keV}}(\mathrm{erg\,s^{-1}})] > 42$.

In our analysis, we used the X-ray dataset used in Mountrichas et al. (2022c). Specifically, we used the same strict photometric selection criteria to make sure that only sources with the best photometric coverage were included in our analysis (u, g, r, i, z, J, H, K_s, IRAC1, IRAC2, and MIPS/24, where IRAC1, IRAC2, and MIPS/24 are the [3.6] µm, [4.5] µm, and 24 µm photometric bands of *Spitzer*). We also applied the same reliability requirements with those described in Sect. 3.2 in Mountrichas et al. (2022c) to make certain that the analysis would be restricted to the sources with the most reliable host galaxy properties (see Sect. 3). We also only used sources that meet the mass completeness limits, as described in detail in Sects. 2.1, 3.2, and 3.4 in Mountrichas et al. (2022c). Specifically, for the redshift range spanned by the sample, the stellar mass completeness limits are $\log[M_{*,95\%\mathrm{lim}}(M_\odot)] = 9.13$ and 9.44 at $0.5 < z < 1.0$ and $1.0 < z < 1.5$, respectively. There are 1161 X-ray sources that meet all the above selection criteria (Table 2 in Mountrichas et al. 2022c).

One goal of this study is to examine the SFRs of galaxies that host AGNs in different cosmic environments. Yang et al. (2018) used sources in the COSMOS field, at $0.3 < z < 3.0$ and studied the dependence of the black hole growth on the cosmic environment. For that purpose, they adopted the 'weighted adaptive kernel smoothing' method to construct the surface-density field that probes sub-Mpc (Megaparsec) physical scales (Darvish et al. 2015). The method was applied to all sources in the COSMOS field, that is, for both non-AGN galaxies and X-ray systems. The end product of this analysis is the calculation of the dimensionless overdensity parameter ($1 + \delta = \frac{\Sigma}{\Sigma_\mathrm{median}}$, where Σ is the surface number density, in units of Mpc^{-2}, and Σ_median is the median Σ at each redshift). The method is described in detail in Sect. 2.3.1 in Yang et al. (2018; see also Darvish et al. 2015). Based on the density field estimates, the cosmic web was then, extracted using the multiscale environment filter (MMF) algorithm (e.g., Aragón-Calvo et al. 2007; Darvish et al. 2014, 2017). The main idea was to measure the geometry of the density field around each point at each redshift. If the geometry was found to be similar to that of a typical cluster or filament, then the point's environment was correspondingly classified as a cluster or filament. Otherwise, the point was classified as the field (for more details, see Sect. 2.3.2 in Yang et al. 2018).

To add the information about the field density and cosmic environment to our X-ray sources, we crossmatched the 1161 sources with the catalogue used in Yang et al. (2018). This resulted in 1005 X-ray AGNs. The missing AGNs (1161 vs. 1005) are due to the fact that in Yang et al. (2018), they filtered out sources near (<1 Mpc) the edge of the field, since the density measurements for these sources are unreliable (see also Darvish et al. 2017).

2.2. The galaxy control sample

The main goal of this work is to compare the SFRs and SFHs of AGN host galaxies in different cosmic environments with the SFRs of non-AGN systems in similar density fields. To this end, we used the galaxy control sample presented in Mountrichas et al. (2022c; see their Sect. 2.2). We applied the same selection criteria used for the X-ray dataset and the same mass completeness limits, which resulted in 89 375 sources

(Table 2 in Mountrichas et al. 2022c). We note that X-ray sources have been excluded from the galaxy control sample, as well as sources with a strong AGN component, calculated by the SED fitting (see next section and Sect. 3.3 in Mountrichas et al. 2022c). To include information about the cosmic environment of the sources in the galaxy control sample, we crossmatched the control sample with the catalogue presented in Yang et al. (2018). There are 76 251 common sources between the two datasets.

3. Galaxy properties

In this section, we describe how we obtained information about the properties of the sources used in our analysis. Specifically, we present how we measured the SFR and M_* of AGN and non-AGN galaxies and how we retrieved knowledge on their stellar populations and morphology.

3.1. Calculation of SFR and M_*

The (host) galaxy properties of both the X-ray AGNs and the galaxies in the control sample were calculated via SED fitting using the CIGALE code (Boquien et al. 2019; Yang et al. 2020, 2022). The SED fitting analysis is described in detail in Sect. 3.1 in Mountrichas et al. (2022c). In brief, the galaxy component was modelled using a delayed SFH model with a function form SFR $\propto t \times \exp(-t/\tau)$. A star formation burst was included (Ciesla et al. 2017; Małek et al. 2018; Buat et al. 2019) as a constant ongoing period of star formation of 50 Myr. Stellar emission was modelled using the single stellar population templates of Bruzual & Charlot (2003) and was attenuated following the Charlot & Fall (2000) attenuation law. To model the nebular emission, CIGALE adopts the nebular templates based on Inoue (2011). The emission of the dust heated by stars was modelled based on Dale et al. (2014), without any AGN contribution. The AGN emission was included using the SKIRTOR models of Stalevski et al. (2012, 2016). CIGALE has the ability to model the X-ray emission of galaxies. In the SED fitting process, we used the observed L_X in the 2−10 keV band provided by Marchesi et al. (2016). The parameter space used is shown in Table 1 in Mountrichas et al. (2022c). The reliability of the SFR measurements, both in the case of AGN and non-AGN systems, was examined in detail in our previous works, in particular in Sect. 3.2.2 of Mountrichas et al. (2022c).

In Mountrichas et al. (2021, 2022a,c), we found that the $\mathrm{SFR_{norm}}-L_X$ relation depends on the stellar mass range probed by the sources. Specifically, a flat $\mathrm{SFR_{norm}}-L_X$ relation was found for the least and most massive systems ($\log[M_*(M_\odot)] < 10.5$ and $\log[M_*(M_\odot)] > 11.5$), with $\mathrm{SFR_{norm}} \sim 1$. Albeit, for intermediate stellar masses ($10.5 < \log[M_*(M_\odot)] < 11.5$), $\mathrm{SFR_{norm}}$ was found to be $\mathrm{SFR_{norm}} \leq 1$ at low-to-moderate L_X ($\log[L_{X,2-10\,keV}(\mathrm{erg\,s^{-1}})] < 44$), whereas at higher L_X, $\mathrm{SFR_{norm}} > 1$ (e.g., see Fig. 5 in Mountrichas et al. 2022a). Amongst the 1005 X-ray AGNs in our dataset, ∼80% (809 sources) have $10.5 < \log[M_*(M_\odot)] < 11.5$. Therefore, there are not enough sources to probe lower or higher M_* in a statistically robust manner. Thus, we restricted our analysis to AGNs (and galaxies) with $10.5 < \log[M_*(M_\odot)] < 11.5$. Furthermore, sources in our datasets (AGNs and non-AGNs) associated with filaments or the field span redshifts up to 2.5. Nevertheless, in our samples, sources in clusters lie at $z < 1.2$. To make sure that our results and conclusions are not affected by the different redshift ranges probed by sources in different cosmic environments, we also restricted both our AGN and non-AGN datasets to $z < 1.2$. There are 551 (430 of which are with spec-z) X-ray AGNs and 16 917 (6653 of which are with spec-z) non-AGN galaxies that met these two criteria (M_*, redshift). Among them, 31 (1048) AGNs (non-AGNs) are associated with clusters, 328 (9622) AGNs (non-AGNs) are associated with filaments, and 192 (6247) AGNs (non-AGNs) are in the field. The distribution of AGNs in the L_X–redshift plane is presented in Fig. 1. These sources were used in the analysis presented in Sect. 4.1.

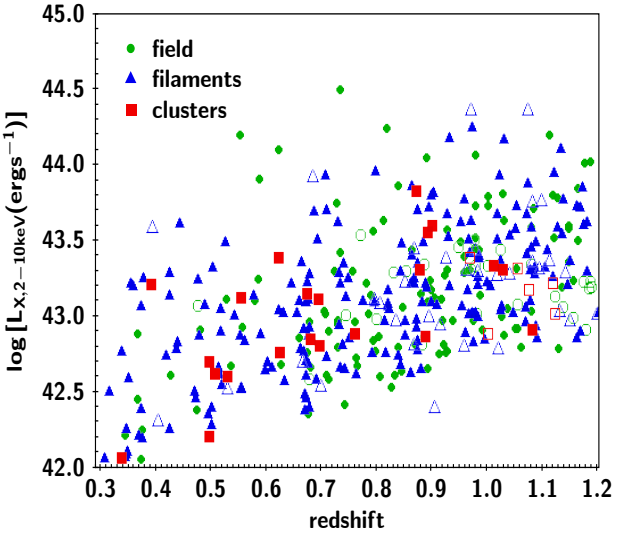

Fig. 1. Distribution of the 551 X-ray AGNs in the L_X–redshift plane. Different colours and symbols correspond to sources associated with different cosmic environments as indicated in the legend. The open symbols represent AGNs with photo-z.

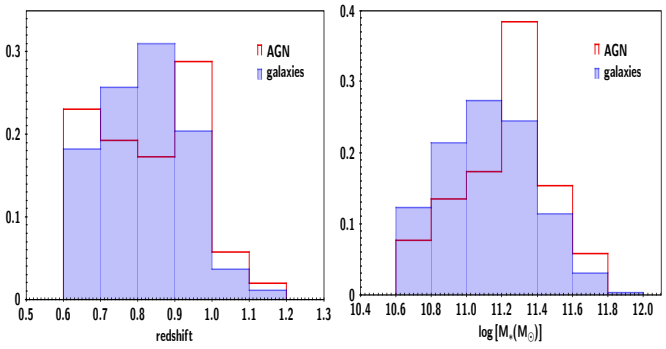

Fig. 2. Distributions of galaxy properties for the 52 AGN (red histograms) and 1172 non-AGN galaxies (blue-shaded histograms) used to study the SFHs of the two populations. Left panel: distribution of redshift. Right panel: distribution of M_*.

3.2. Star formation history

In Mountrichas et al. (2022b), we examined the SFHs of AGN and non-AGN galaxies, and we found that AGNs of low-to-moderate L_X ($\log[L_{X,2-10\,keV}(\mathrm{erg\,s^{-1}})] < 44$) tend to have older stellar populations and are less likely to have experienced a recent star formation burst compared to non-AGN systems. In this work, we not only study the SFHs of the two populations but also take into account their cosmic environment (Sect. 4.2). For that purpose, we crossmatched our AGNs and galaxies in the control sample with the LEGA-C catalogue (van der Wel et al. 2016, 2021; Straatman et al. 2018). This catalogue includes spectra for 4081 galaxies (3741 unique objects) within $0.6 < z < 1.3$.

We made use of two tracers that are sensitive to stellar age and are available in the LEGA-C dataset. These tracers are the equivalent width (EW) of H_δ absorption and the D_n4000 index (e.g., Kauffmann et al. 2003; Wu et al. 2018). The D_n4000 is small for young stellar populations and large for old metal-rich galaxies. On the other hand, the EW of H_δ rises rapidly in the first few hundred million years after a burst of star formation, when O- and B-type stars dominate the spectrum, and then decreases when A-type stars fade (e.g., Kauffmann et al. 2003; Wu et al. 2018).

We applied the same quality selection criteria described in Sect. 2.2.3 in Mountrichas et al. (2022b), which reduced the number of sources in the LEGA-C catalogue to 2834. Then, we crossmatched our X-ray and galaxy control samples with the LEGA-C dataset. This resulted in 52 AGN and 1172 non-AGN galaxies. The average uncertainties on H_δ and D_n4000 are 17% and 3%, respectively. We note that the control sample was reduced to those sources with $\log[M_*(M_\odot)] > 10.6$ to better match the M_* range of the X-ray dataset. The redshift and M_* distributions of the two populations are shown in Fig. 2. Both distributions are similar between the two populations. A Kolmogorov–Smirnov (KS) test gave a p-value of 0.57 and 0.12 for the redshift and M_* distributions of AGN and non-AGN galaxies, respectively (the two distributions differ with a statistical significance of $\sim 2\sigma$ for a p-value of 0.05). Similar values were found when applying a Mann-Whitney test (p-value of 0.90 and 0.29, respectively, for the redshift and M_* distributions). Therefore, we considered that the M_* and redshift distributions of AGN and non-AGN galaxies are not significantly different to affect the results presented in Sect. 4.2. Nevertheless, we confirm that if we account for the (small) differences in the redshift and M_* distributions of the two populations following the methodology described in Mountrichas et al. (2019, 2022b), Masoura et al. (2021), Buat et al. (2021), for example (i.e., weigh the sources based on their M_* and redshift), it does not change our results and overall conclusions.

3.3. Morphology

To examine the role of the morphology of AGN and non-AGN galaxies in different cosmic environments (see Sect. 4.3), we used the catalogue presented in Ni et al. (2021). The morphological classification was done using a deep learning-based method to separate sources into BD and non-BD galaxies. The term BD refers to galaxies that only display a significant spheroidal component without obvious disc-like or irregular components (for more information, see Appendix C and Sect. 2.3 in Ni et al. 2021; Yang et al. 2019, respectively).

We crossmatched the datasets described in Sect. 3.2 with the catalogue of Ni et al. (2021), which resulted in 37 AGN and 1086 non-AGN galaxies. Type 1 AGNs were removed from the Ni et al. (2021) sample since they can potentially affect host galaxy morphological measurements (see their Sect. 2.4). We also note that the redshift and M_* distributions of AGN and non-AGN galaxies used in this part of our analysis are very similar to those presented in Fig. 2, and thus we assumed that the small differences in the redshift and M_* distributions of the two populations do not affect our results.

4. Results

In this section, we compare the SFRs of AGN and non-AGN galaxies as a function of the L_X for different cosmic environments. We also examine if the results of this comparison are affected by the exclusion of Q systems from both populations. Furthermore, we study the SFHs of the two populations for different density fields. Finally, we compare the effect of morphology and environment on the stellar populations of AGN and non-AGN systems.

4.1. Comparison of the star formation rate of AGN and non-AGN galaxies as a function of L_X and cosmic environment

First, we compare the SFRs of AGN host galaxies with the SFRs of non-AGN systems as a function of the cosmic environment. For this purpose, we used the SFR_{norm} parameter. The SFR_{norm} is defined as the ratio of the SFRs of galaxies that host AGNs to the SFRs of non-AGN systems with similar M_* and redshift (e.g., Mullaney et al. 2015; Masoura et al. 2018, 2021; Bernhard et al. 2019; Mountrichas et al. 2021, 2022a,c). For the estimation of SFR_{norm}, we used the X-ray and galaxy control samples described in Sect. 2. The SFR_{norm} was measured following the process of our previous studies (e.g., Mountrichas et al. 2021, 2022a,c). Specifically, the SFR of each X-ray AGN was divided by the SFRs of galaxies in the control sample that are within ± 0.2 dex in M_*, $\pm 0.075 \times (1+z)$ in redshift and are in similar density fields. Furthermore, each source was weighted based on the uncertainty of the SFR and M_* measurements made by CIGALE. Then, the median values of these ratios were used as the SFR_{norm} of each X-ray AGN. We note that our measurements are not sensitive to the choice of the box size around an AGN. Selecting smaller boxes, though, has an effect on the errors of the calculations (Mountrichas et al. 2021).

The top panel of Fig. 3 presents the SFR_{norm} as a function of L_X for different cosmic environments. Measurements are the median values of SFR_{norm} grouped in bins of L_X of size 0.5 dex. The errors presented are 1σ, calculated using bootstrap resampling (e.g., Loh 2008). Only bins that have more than ten sources are presented. We note that the $SFR_{norm}-L_X$ relation is flat for sources found in the field. However, an increase of SFR_{norm} was observed, in particular at $\log[L_{X,2-10\,keV}(erg\,s^{-1})] > 43$, for sources associated with filaments and clusters. This implies that for X-ray luminosities probed by our dataset, AGNs in the field have lower SFRs compared to the SFRs of non-AGN systems, regardless of the L_X. However, in denser environments, the SFRs of AGNs compared to non-AGN galaxies depends on the L_X. At $\log[L_{X,2-10\,keV}(erg\,s^{-1})] < 43$, as AGNs appear to have lower SFRs compared to non-AGN, whereas at moderate L_X, AGNs have similar or larger SFRs compared to non-AGN systems. Previous studies (Mountrichas et al. 2022a,c) have found that the SFRs of low-to-moderate L_X AGNs (i.e., $\log[L_{X,2-10\,keV}(erg\,s^{-1})] < 44$) are lower, or at most equal to, the SFRs of non-AGN systems. In light of our current measurements, these previous results could be attributed to the density field of the sources. That is, low-to-moderate L_X AGNs have lower SFRs compared to non-AGN systems when both populations are found in the field, but the SFRs of (moderate L_X) X-ray AGNs are similar to or larger than that of non-AGN galaxies when the sources are associated with filaments or clusters.

We repeated the same exercise presented above, but we instead classified AGNs and non-AGNs by using their overdensity values. Specifically, the sources that have overdensity values that belong to the highest 20% of the total samples were classified as sources in 'high-density fields', whereas those with overdensity values that belong to the lowest 20% of the total samples were characterised as sources in 'low-density fields'. Sources that belong to the high-density field group have $\log(1+\delta) > 0.28$

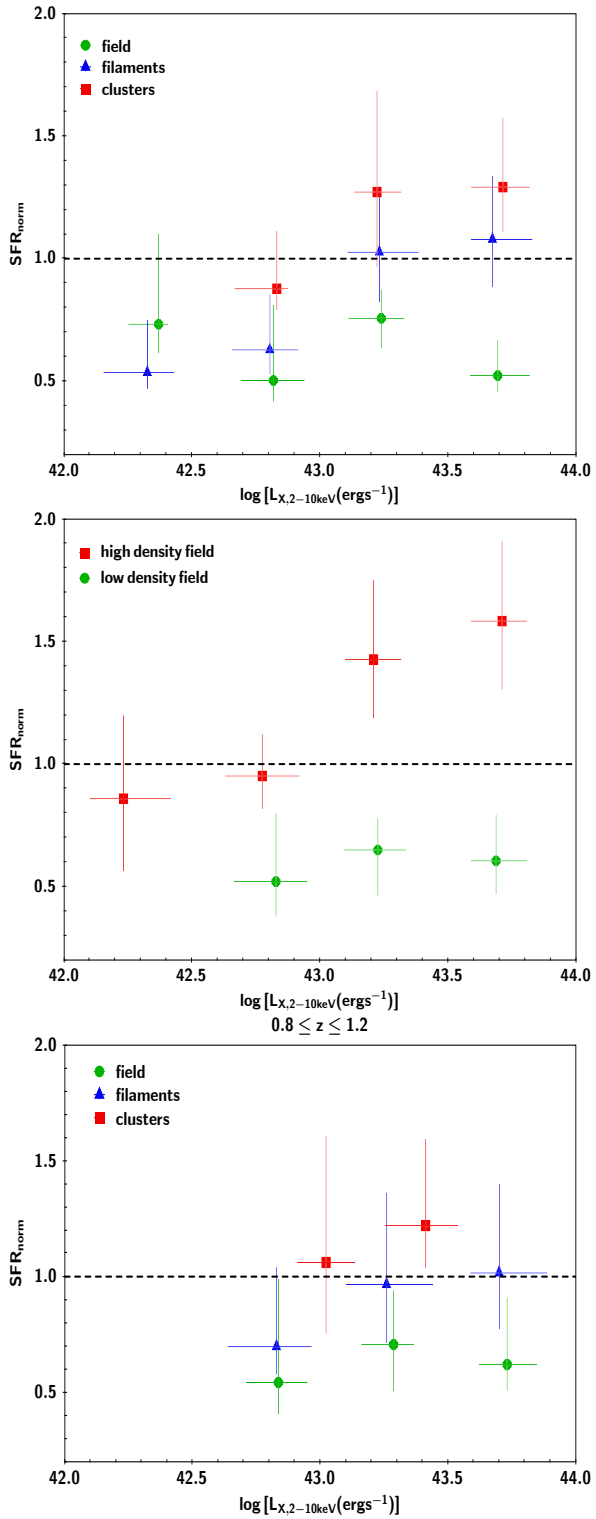

Fig. 3. Median values of $\mathrm{SFR_{norm}}$ $\left(=\frac{\mathrm{SFR_{AGN}}}{\mathrm{SFR_{non\text{-}AGN}}}\right)$ as a function of L_X. The measurements are grouped in bins of L_X of 0.5 dex width. The errors presented are 1σ, calculated using bootstrap resampling. Top panel: results when we classified sources based on their cosmic environment, as indicated in the legend. Middle panel: results when sources are classified using their overdensity values (see text for more details). Bottom panel: similar to the top panel, but we restricted our dataset to $0.8 \leq z \leq 1.2$.

(both in the case of AGN and non-AGN galaxies), whereas those in the low-density field group have $\log(1+\delta) < -0.12$. The $\mathrm{SFR_{norm}}$ as a function of the L_X for the two classes is presented in the middle panel of Fig. 3. These results confirmed our previous observations, but the trends are now more clear and appear statistically significant. Specifically, the $\mathrm{SFR_{norm}}$ in denser fields is higher compared to fields of low density, with a $\sim 2\sigma$ significance level, and there is an increase of $\mathrm{SFR_{norm}}$ with L_X for sources in dense environments, whereas in fields of low density, the $\mathrm{SFR_{norm}}-L_X$ relation is flat, and the $\mathrm{SFR_{norm}}$ is consistently less than one (i.e., the SFRs of AGNs are lower compared to the SFRs of non-AGN galaxies).

To examine if our results are affected by possible evolution with cosmic time within the redshift range that our datasets span ($0.3 < z < 1.2$), we restricted our samples to a narrow redshift interval, that is, $0.8 \leq z \leq 1.2$. There are 238 AGNs and 8019 sources in the control sample within this redshift range. The results using these subsets are presented in the bottom panel of Fig. 3. The statistical uncertainties are larger due to the smaller size of the subsets used, but the same trends were observed with those using the sources within the wider redshift interval.

Next, we examine if the trends observed above for the total AGN and non-AGN galaxies hold in the case of star-forming sources, that is, after excluding Q systems. In our previous studies (Mountrichas et al. 2021, 2022c,a), we identified Q systems (both AGN and non-AGN galaxies) by using their specific SFR measurements ($\mathrm{sSFR} = \frac{SFR}{M_*}$), and we excluded them from our analysis when studying the $\mathrm{SFR_{norm}}-L_X$ relation. Therefore, for this work, we used systems identified as Q in Mountrichas et al. (2022c; see their Sect. 3.5) that studied the $\mathrm{SFR_{norm}}-L_X$ in the COSMOS field, and we examined whether their fraction differs between AGN and non-AGN galaxies in different cosmic environments. We found that the fraction of Q sources increases in denser fields for non-AGN galaxies from ~25% for isolated galaxies (or galaxies in low-density fields) to ~40% in the most dense environments. In the case of AGNs, the fraction of Q systems is similar in all environments (~30%).

Next, we repeated the $\mathrm{SFR_{norm}}-L_X$ measurements but excluded Q systems. The results are presented in Fig. 4. We note that due to the smaller size of these samples, there is only one bin that satisfied our requirement for the minimum number of sources (>10) in the case of AGNs in clusters. Overall, when Q systems are not included in the analysis, the amplitude of the $\mathrm{SFR_{norm}}$ is lower (by ~0.2 dex) for all cosmic environments and for the L_X spanned by our datasets compared to the $\mathrm{SFR_{norm}}$ values derived using the total samples (Fig. 3). However, the trends mentioned earlier remain unchanged. Specifically, the $\mathrm{SFR_{norm}}$ is higher for denser environments, and an increase of $\mathrm{SFR_{norm}}$ with L_X was observed for sources associated with filaments or clusters.

4.2. The star formation histories of AGN and non-AGN galaxies as a function of the cosmic environment

In this section, we study the SFHs of AGN and non-AGN galaxies. Our goal is to check whether their stellar populations agree with the picture drawn in Sect. 4.1 (i.e., systems with lower SFRs are expected to have older stars compared to systems with higher SFRs). Moreover, the study of the SFHs could allow us to uncover what drives the trends we observed in the previous section. We note that the selection of sources with available D_n4000 and H_δ measurements does not bias our samples against Q systems. In other words, the AGN and non-AGN datasets used in this part of our analysis include the same fraction of Q systems with the datasets used in the previous section. Therefore, a direct comparison can be made regarding the results of these two parts of our analysis.

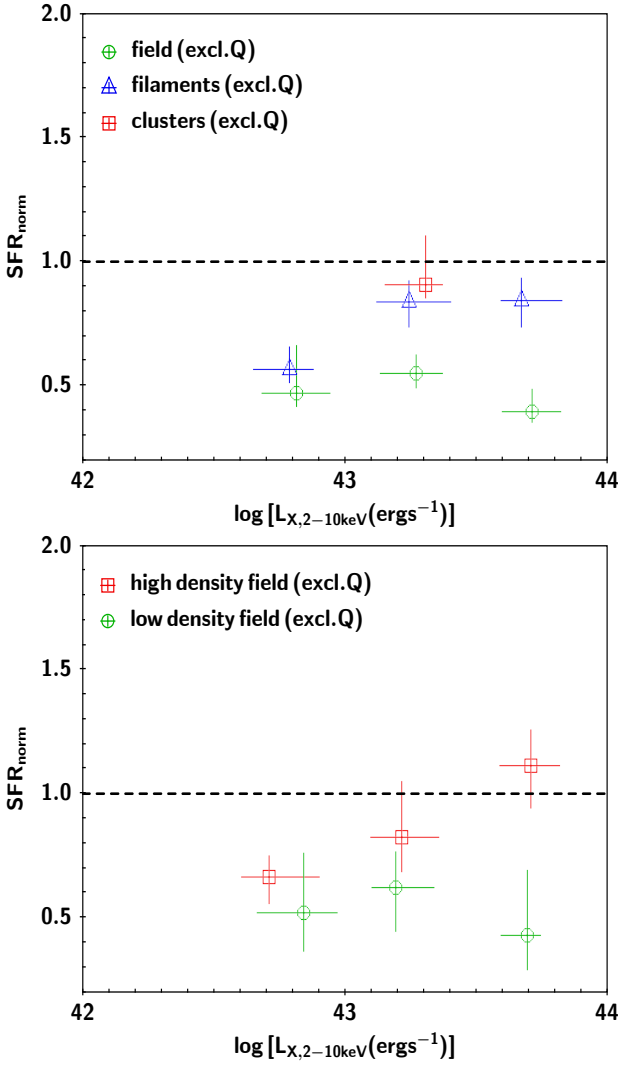

Fig. 4. Same as Fig. 3 but excluding quiescent (Q) systems both from the AGN and galaxy samples.

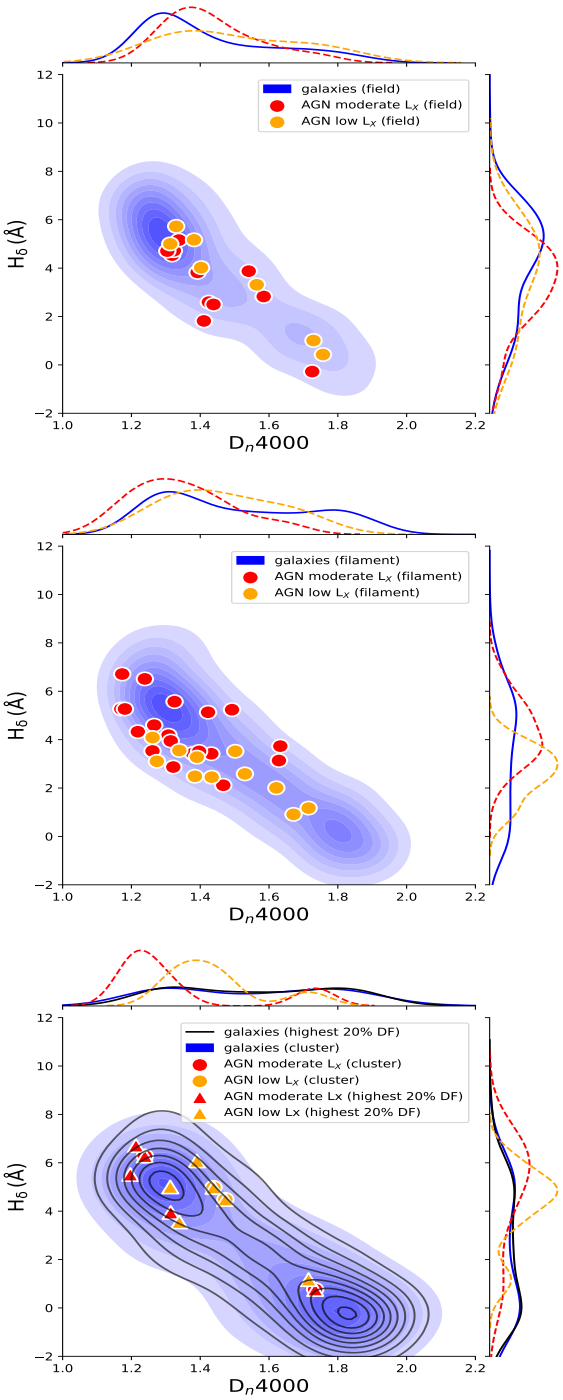

Fig. 5. Distributions in the H_δ–D_n4000 space of non-AGN galaxies (blue-shaded contours) and low ($\log[L_{X,2-10\,keV}(erg\,s^{-1})] < 43$; orange circles) and high ($43 < \log[L_{X,2-10\,keV}(erg\,s^{-1})] < 44$; red circles) L_X AGNs for different cosmic environments. Top panel: Distribution of isolated sources (field). Middle panel: distribution of sources associated with filaments. Bottom panel: distribution of sources found in the most dense fields. See text for more details.

Figure 5 presents the distributions of AGN and non-AGN galaxies in the H_δ–D_n4000 space for sources in the field (top panel) and those associated with filaments (middle panel) and clusters (bottom panel). Prompted by the results in the previous section, we split our AGNs into two L_X bins at $\log[L_{X,2-10\,keV}(erg\,s^{-1})] = 43$. The red circles indicate AGNs with $\log[L_{X,2-10\,keV}(erg\,s^{-1})] > 43$ ('moderate L_X'), and orange circles represent AGNs with $\log[L_{X,2-10\,keV}(erg\,s^{-1})] < 43$ ('low L_X'). The number of available AGNs and non-AGNs are presented in Table 1.

Regarding the D_n4000 and H_δ distributions for AGN and non-AGN galaxies that are in the field (top panel of Fig. 5), we noticed that the two AGN populations have similar stellar ages and are higher compared to non-AGN systems. A KS test yielded a p-value of approximately one for the D_n4000 distributions of low and moderate L_X AGNs. Comparing the distributions between AGN and non-AGN galaxies, we obtained a p-value of 0.20 and 0.008 for the D_n4000 distributions of moderate and low L_X AGNs compared to non-AGN systems, which indicates a statistically significant difference, at least in the case of low L_X AGNs compared to non-AGNs. The AGNs also tend to have lower H_δ values compared to sources in the control sample. However, based on a KS test, this difference does not appear to be statistically significant. Merging the two AGN populations and comparing their H_δ and D_n4000 distributions with those of their non-AGN counterparts does not affect the overall results. Specifically, AGNs appear to have higher D_n4000 and lower H_δ values compared to non-AGN galaxies. Based on the p-values of the KS tests, the first difference is statistically significant (p-value of 0.02 and 0.05, respectively, for D_n4000 and H_δ).

The above results suggest that AGNs that live in the field tend to have older stellar populations and are less likely to have experienced a recent star formation burst compared to isolated non-AGN systems. These results are in agreement with those presented in Fig. 3. The picture that emerges is that AGNs that are in the field have similar SFRs and SFHs regardless of the AGN power (L_X) and have, on average, lower SFRs and older stellar ages compared to their non-AGN field counterparts.

On the other hand, as shown in the middle panel of Fig. 5, AGNs that live in denser environments (i.e., filaments) have different SFHs depending on their L_X. Specifically, AGNs with $\log[L_{X,2-10\,keV}(erg\,s^{-1})] > 43$ tend to have lower D_n4000 (= 1.32 vs. = 1.44) and higher H_δ values (= 4.20 vs. = 2.56) compared to their lower L_X counterparts (p-value of ∼0.3 for both spectral indices). These differences, although not statistically significant based on KS tests, are in agreement with the results we found in the previous section, where higher L_X AGNs have increased SFR_{norm} compared to lower L_X sources. Regarding the non-AGN galaxies, they appear to have flatter D_n4000 and H_δ distributions compared to AGNs (median $D_n4000 = 1.46$, $H_\delta = 3.46$).

Finally, the bottom panel of Fig. 5 presents the D_n4000 and H_δ distributions for AGN and non-AGN systems that are associated with the most dense cosmic environments. Since there are only four AGNs that live in clusters in our dataset, we followed the same approach we used in the previous section. That is, we also classified sources based on their overdensity values. We note that the results are very similar for both the D_n4000 and the H_δ of the non-AGN galaxies regardless of whether the classification is based on the cosmic environment (clusters) or the overdensity value (i.e., the solid black and red lines). The AGNs with $\log[L_{X,2-10\,keV}(erg\,s^{-1})] > 43$ have lower D_n4000 and higher H_δ values compared to their lower L_X counterparts (p-value of 0.00003 and 0.004 for D_n4000 and H_δ, respectively) and the non-AGN galaxies (p-value of 0.02 and 0.006 for D_n4000 and H_δ, respectively). Based on the p-values of the KS tests, these differences are statistically significant at a level of $>2\sigma$. This confirms our findings presented in the previous section of higher SFRs for high L_X AGNs compared to lower L_X X-ray sources and non-AGN systems.

Table 1 shows the median D_n4000 and H_δ values for the different populations and cosmic environments. Non-AGN galaxies tend to have higher D_n4000 and lower H_δ values when moving to denser fields, which indicates that their stellar population becomes older in denser environments and is in agreement with most previous studies (e.g., Pérez-Millán et al. 2023). In addition to the median values presented in Table 1, there are noteworthy differences in the D_n4000 and H_δ distributions of galaxies in different cosmic environments (Fig. 5). For galaxies in the field, the two distributions present a long tail. This tail becomes more prominent for sources associated with filaments, and in the case of galaxies in the densest environments, the distributions become flat. We confirmed that these long tails (secondary peaks) are populated, mainly, by Q galaxies, and their prominence is associated with the increased fraction of Q non-AGN systems in denser environments.

On the other hand, AGNs, and in particular X-ray sources with $\log[L_{X,2-10\,keV}(erg\,s^{-1})] < 43$, have consistent H_δ and, especially, D_n4000 values in all cosmic environments (Table 1). Their D_n4000 and H_δ distributions have less prominent tails compared to non-AGN galaxies (Fig. 5). More luminous AGNs show a tendency of lower D_n4000 and higher H_δ values in the most dense environments, although the sub-sample is small and larger datasets are required to confirm these findings.

These results can provide an explanation as to what drives the trends we observed in the previous section. Specifically, the increase of the SFR_{norm} as we moved from the field to filaments and to clusters (Fig. 3) is mainly driven by the lower SFRs of galaxies in higher density fields and, to a lesser degree, is due to the increased SFRs of the more luminous AGNs in denser cosmic environments.

We repeated the same exercise, but this time we separated the sources into star-forming systems and Q systems. The results are shown in Table 2. Due to the small number of available AGNs, we did not split the AGNs based on their L_X. We also characterised the cosmic environment of sources based on their overdensity values (see Sect. 4.1). The results show that the stellar populations of Q systems, both in the case of AGN and non-AGN galaxies, depend on the cosmic environment, whereas for star-forming systems, the differences with the density field are smaller. We note, however, that in the case of AGNs, the measurements come from a small number of sources in each density field. Specifically, both at high and low-density fields, our AGN subsamples include eight star-forming systems and three Q systems.

4.3. Environment versus morphology

In this section, we examine the morphology of AGN and non-AGN galaxies in different cosmic environments. This allows us to study the SFHs of AGN and non-AGN systems in different environments but with a fixed morphological type. It also enables us to examine the link between morphology (e.g., BD) and galaxy phase (e.g., Q) for the two populations.

There are nine (24%) AGNs in our dataset that live in BD systems. A similar fraction (21%) of BD galaxies was also found in the non-AGNs sample. We also note that the fraction of Q systems is similar (∼40%) for AGN and non-AGN galaxies. We found similar fractions between the AGNs and the galaxies in the control sample to be associated with fields, filaments, and clusters (see Table 3). A noteworthy difference, though, is that the percentage of BD systems shows an increase (albeit mild) towards higher density environments amongst the non-AGN galaxies, similar to the increase of the fraction of Q systems in denser fields. In contrast, the percentage of BD systems that also host AGNs is significantly reduced in AGNs associated with dense cosmic environments, while the fraction of Q AGN hosts remains roughly the same, independent of the density field. When we associated sources with high-density regions based on the overdensity values of the sources, the fractions of BD systems in both the AGN and the non-AGN datasets (numbers in square brackets in Table 3) is the same as those we found using their cosmic environment, and therefore the same conclusions were reached.

Thus, based on our analysis, BD systems are nearly equally likely to be found in non-AGN galaxies regardless of their cosmic environment. In the case of galaxies that host (type 2) AGNs, BD systems are preferentially found in AGNs associated with less dense fields. Moreover, the link between morphology (BD) and galaxy phase (Q) is weaker for AGNs compared to non-AGN galaxies. This was confirmed by the study of the stellar populations, presented in Table 3. The stellar population of non-AGN galaxies is different for BD and non-BD systems as compared to galaxies that host AGNs, in which case smaller differences are observed in the stellar populations for different morphologies (see also Mountrichas et al. 2022b). We note, however, that in the case of AGNs, the size of the available dataset is small, and larger samples are required to confirm our findings.

Table 1. Number of X-ray AGNs and sources in the control sample with available D_n4000 and H_δ measurements from the LEGA-C catalogue in different cosmic environments.

	Field		Filament		Cluster	
L_X (erg s^{-1})	$<10^{43}$	$\geq10^{43}$	$<10^{43}$	$\geq10^{43}$	$<10^{43}$	$\geq10^{43}$
No. AGN	7	11	11	19	2 (6)	2 (5)
D_n4000, H_δ (AGN)	1.40, 4.00	1.41, 3.89	1.44, 2.56	1.32, 4.20	1.44, 4.95	1.22, 5.53
No. galaxies	490		603		79 (244)	
D_n4000, H_δ (galaxies)	1.36, 4.45		1.46, 3.46		1.55, 2.23	

Notes. The median D_n4000 and H_δ values of each subset are also presented. The numbers in parentheses show the number of AGNs when we classified sources using their overdensity values (see text for more details).

Table 2. Median D_n4000 and H_δ values for star-forming and Q AGN and non-AGN galaxies in different density fields.

	Low-density field		High-density field	
	SF	Q	SF	Q
D_n4000, H_δ (AGN)	1.31, 4.18	1.44, 0.27	1.34, 4.98	1.72, 1.17
D_n4000, H_δ (galaxies)	1.30, 5.13	1.67, 1.74	1.35, 1.78	1.78, 0.21

Table 3. Number of X-ray AGNs and sources in the control sample for different morphologies and cosmic environments.

	Field		Filament		Cluster	
Morphology	BD	Non-BD	BD	Non-BD	BD	Non-BD
No. AGN	12 (32%)		21 (57%)		4 (11%)	
AGN	6(50%)	6(50%)	3(14%)	18(86%)	0(0%) [0(0%)]	4(100%) [13(100%)]
D_n4000, H_δ (AGN)	1.58, 5.00	1.40, 4.54	1.63, 2.58	1.42, 3.43	nan, nan	1.47, 4.98
No. galaxies	494(41%)		560(53%)		72(7%) [218]	
Galaxies	87(19%)	367(81%)	121(22%)	439(78%)	20(28%) [62(28%)]	52(72%) [156(72%)]
D_n4000, H_δ (galaxies)	1.67, 1.23	1.32, 5.03	1.76, 0.64	1.38, 4.19	1.80, −0.04	1.40, 3.62

Notes. The median D_n4000 and H_δ values of each subset are also presented. The numbers in the square brackets show the number of AGNs when we classified sources using their overdensity values (see text for more details).

5. Discussion

Previous galaxy studies that examined the role of the cosmic environment and morphology on star formation have found controversial results. For instance, Erfanianfar et al. (2016), used X-ray-selected galaxy groups and found a mild dependence of star formation on the environment at $0.5 < z < 1.1$ for main-sequence galaxies. Their findings suggest that stellar mass, morphology, and environment act together in moving the star formation to lower levels. However, environmental effects are more prominent at lower redshifts. Darvish et al. (2016) studied star-forming and Q galaxies in the COSMOS field at $z \leq 3$. They found that star-forming galaxies have similar SFRs and sSFR in different environments regardless of their redshift and M_*. The fraction of Q systems depends on the environment at $z \leq 1$ and on M_* out to $z \sim 3$. Moreover, galaxies at $z \leq 1$ become Q faster in denser environments, and the overall environmental quenching efficiency increases with cosmic time. They also concluded that environmental and mass quenching processes depend on each other, and they become prominent at different cosmic times. Specifically, environmental quenching is only relevant at $z \leq 1$, whereas mass quenching is the dominant mechanism at $z \geq 1$. Leslie et al. (2020) used galaxies in the COSMOS field and found no variations in the main sequence in different environments. Albeit, they found that BD galaxies have lower SFRs than disc-dominated galaxies at fixed M_* at $z < 1.2$. Delgado et al. (2022) studied galaxy members in 80 groups at $z \leq 0.8$ and found, amongst other results, that the fraction of red and Q galaxies is always higher in groups than in the field. More recently, Cooke et al. (2023) used star-forming galaxies in the COSMOS field and found no environmental or morphological dependence related to the shape of the main sequence up to a redshift of 3.5. Pérez-Millán et al. (2023) performed a detailed study on the dependence of the observed galaxy properties on M_*, morphology, and environment and found that at a fixed M_* and morphology, clusters have higher quenching efficiencies. They concluded that the cluster environment affects the ability to form stars, independent of morphological type. Sobral et al. (2022) used the LEGA-C catalogue and the local overdensities estimated by Darvish et al. (2015, 2017) and found that the fraction of Q galaxies hinges on M_* and on the environmental density. Their findings also showed that the D_n4000 and H_δ indices of galaxies depends on M_* and on the cosmic environment, particularly in the case of Q galaxies, whereas for star-forming systems, the two spectral indices depend, mainly, on M_* and do not show a significance dependence on environment. They concluded that Q galaxies in higher density fields are older and are formed and/or quenched earlier.

Our analysis shows that galaxies with $\log[M_*(M_\odot)] > 10.6$ at $z \sim 1$ have different stellar populations in different cosmic environments (Table 1), and these differences are mainly driven by Q (or BD) systems (Tables 2 and 3), which is in agreement

with, for instance, Sobral et al. (2022). Our results also show that galaxy morphology is affected by the environment, with the fraction of BD systems to increase with the density field (see also, e.g., Dressler 1980; Fasano et al. 2015). Recently, Hasan et al. (2023) analysed outputs from the Illustris-TNG-100 magneto-hydrodynamical cosmological simulations (Pillepich et al. 2018; Nelson et al. 2019). Their analysis showed that the influence of the cosmic environment on star-formation activity starts at $z \sim 2$ and that most of the star formation-environment relationships can be explain in terms of the evolution of the median gas fraction. Specifically, the quenching of star formation in dense environments is due to rapid gas stripping or, in the case of intermediate density fields, due to gradual gas starvation.

The main focus of this work is on the role of the SMBH activity in the star formation and stellar population of galaxies in different environments (and morphologies). Our results show that galaxies that host low-luminosity AGNs ($\log[L_{\rm X,2-10\,keV}(\rm erg\,s^{-1})] < 43$) have, on average, consistent stellar populations, independent of the cosmic environment. Their SFRs are also lower compared to the SFRs of non-AGN galaxies ($\rm SFR_{norm} \sim 1$), regardless of the field density. Galaxies that host moderate $L_{\rm X}$ AGNs ($43 < \log[L_{\rm X,2-10\,keV}(\rm erg\,s^{-1})] < 44$) have stellar populations that tend to be younger in denser fields compared to the field. Their SFRs are also similar, if not higher, compared to the SFRs of non-AGN galaxies ($\rm SFR_{norm} \geq 1$). This could imply that the AGN feedback in dense environments counteracts the removal of the gas and prevents the quenching of the star formation (i.e., positive feedback; e.g., Zinn et al. 2013; Santoro et al. 2016; Meenakshi et al. 2022). The higher the AGN activity ($L_{\rm X}$) is, the more efficient the AGN feedback. However, an alternative interpretation of our results could be that a common mechanism (for instance, mergers; e.g., Di Matteo et al. 2005; Hopkins et al. 2008) feeds both the star formation and the SMBH, and triggers the star-formation and the AGN activity (e.g., Bower et al. 2006; Fanidakis 2012). In this scenario, the more gas funnelled to the galaxy due to the triggering mechanism, the higher the increase of the SFR and the AGN power ($L_{\rm X}$). This picture is also consistent with the different morphological types that prevail in different environments between AGN and non-AGN systems. Specifically, the rarity of BD galaxies in systems that host AGNs in dense fields could be an indication of galaxy interactions that trigger both phenomena. Finally, the lower SFRs of galaxies that host AGNs, compared to non-AGN systems ($\rm SFR_{norm} < 1$), in low dense fields could be explained by a low availability of gas in these systems. For instance, Zubovas et al. (2013) showed that in galaxies that are in a gas-poor phase, AGN feedback may quench the star formation process.

6. Conclusions

We studied 551 X-ray AGNs and 16 917 non-AGN galaxies at $0.3 < z < 1.2$ in the COSMOS field, comparing their SFRs ($\rm SFR_{norm}$) as a function of $L_{\rm X}$ in different cosmic environments. We restricted the M_* of both populations to the range of $10.5 < \log[M_*(M_\odot)] < 11.5$. The classification of the sources in three environments (i.e., field, filaments, clusters) is available in the catalogue of Yang et al. (2018). The categorisation is based on their field density, using the method described in Darvish et al. (2015). The (host) galaxy properties were calculated via SED fitting, using the CIGALE code and the measurements presented in Mountrichas et al. (2022c). We crossmatched our datasets with the LEGA-C catalogue, which allowed us to study the SFHs of the two populations for different field densities. This information is available for 52 AGN and 1172 non-AGN galaxies. Finally, we compared the role of the environment versus morphology based on the morphological information in the catalogue of Ni et al. (2021), using 37 AGN and 1086 non-AGN galaxies that are common between the datasets. Our main results can be summarised as follows:

- The SFRs of galaxies that host AGNs is lower compared to the SFRs of non-AGN systems ($\rm SFR_{norm} < 1$) for isolated sources (field) at all $L_{\rm X}$ spanned by our dataset ($42 < \log[L_{\rm X,2-10\,keV}(\rm erg\,s^{-1})] < 44$). However, in denser environments, an increase of $\rm SFR_{norm}$ ($\rm SFR_{norm} \sim 1$) is observed at intermediate $L_{\rm X}$ ($\log[L_{\rm X,2-10\,keV}(\rm erg\,s^{-1})] > 43$).
- The $\rm SFR_{norm}$ appears higher in fields of higher density compared to lower density fields.
- Non-AGN galaxies tend to have older stellar populations (higher D_n4000 values) and are less likely to have undergone a recent star formation burst (lower H_δ values) in denser environments compared to isolated sources (field). In contrast, low $L_{\rm X}$ AGNs have consistent stellar populations (similar D_n4000 and H_δ values) in all cosmic environments, while moderate $L_{\rm X}$ AGNs tend to have younger stars and are more likely to have undergone a recent burst in high-density fields.
- The differences of the stellar populations for different cosmic environments are mainly driven by quiescent systems for both AGN and non-AGN galaxies.
- Although the same fraction of AGN and non-AGN systems is associated with different cosmic environments and the same fraction of BD systems is found for both AGN and non-AGN galaxies, the morphology as a function of the environment is different for the two populations. Specifically, in the case of non-AGN galaxies, the percentage of BD systems increases with the field density, whereas in the case of AGNs, BD systems become scarce in denser environments.

In this work, we studied the SFRs and stellar populations of AGN and non-AGN galaxies in different cosmic environments (and morphologies). Larger samples that include sources observed in wider fields, such as the eFEDS field, would be extremely useful to confirm our findings and expand our investigations to larger M_*, $L_{\rm X}$, and redshift baselines. Previous studies have showcased the importance of M_* when comparing the star formation and stellar populations of AGN and non-AGN systems. Therefore, larger samples that span, in sufficient numbers, lower ($\log[M_*(M_\odot)] < 10.5$) and higher ($\log[M_*(M_\odot)] > 11.5$) M_* are important to examining whether our results change at different M_* regimes. Datasets that cover a wider redshift baseline will also allow for examination of a possible dependence with cosmic time. Finally, as X-ray AGNs used in this study probed low-to-moderate $L_{\rm X}$, it would be particularly interesting to check if and how the results change in the case of the most powerful AGNs ($\log[L_{\rm X,2-10\,keV}(\rm erg\,s^{-1})] > 44$).

Acknowledgements. This project has received funding from the European Union's Horizon 2020 research and innovation program under grant agreement no. 101004168, the XMM2ATHENA project. The project has received funding from Excellence Initiative of Aix-Marseille University – AMIDEX, a French 'Investissements d'Avenir' programme. This work was partially funded by the ANID BASAL project FB210003. M.B. acknowledges support from FONDECYT regular grant 1211000. This research has made use of TOPCAT version 4.8 (Taylor 2005).

References

Aragón-Calvo, M. A., Jones, B. J. T., van de Weygaert, R., & van der Hulst, J. M. 2007, A&A, 474, 315
Bernhard, E., Grimmett, L. P., Mullaney, J. R., et al. 2019, MNRAS, 483, L52

Boquien, M., Burgarella, D., Roehlly, Y., et al. 2019, A&A, 622, A103
Bower, R. G., Benson, A. J., Malbon, R., et al. 2006, MNRAS, 370, 645
Boyle, B. J., Shanks, T., Croom, S. M., et al. 2000, MNRAS, 317, 1014
Brambila, D., Lopes, P. A. A., Ribeiro, A. L. B., & Cortesi, A. 2023, MNRAS, 523, 785
Bruzual, G., & Charlot, S. 2003, MNRAS, 344, 1000
Buat, V., Ciesla, L., Boquien, M., Małek, K., & Burgarella, D. 2019, A&A, 632, A79
Buat, V., Mountrichas, G., Yang, G., et al. 2021, A&A, 654, A93
Charlot, S., & Fall, S. M. 2000, ApJ, 539, 718
Ciesla, L., Elbaz, D., & Fensch, J. 2017, A&A, 608, A41
Civano, F., Marchesi, S., Comastri, A., et al. 2016, ApJ, 819, 62
Cooke, K. C., Kartaltepe, J. S., Rose, C., et al. 2023, ApJ, 942, 49
Dale, D. A., Helou, G., Magdis, G. E., et al. 2014, ApJ, 784, 83
Darvish, B., Sobral, D., Mobasher, B., et al. 2014, ApJ, 796, 51
Darvish, B., Mobasher, B., Sobral, D., Scoville, N., & Aragon-Calvo, M. 2015, ApJ, 805, 121
Darvish, B., Mobasher, B., Sobral, D., et al. 2016, ApJ, 825, 113
Darvish, B., Mobasher, B., Martin, D. C., et al. 2017, ApJ, 837, 16
Das, A., Pandey, B., & Sarkar, S. 2021, J. Cosmol. Astropart. Phys., 2021, 045
Delgado, R. M. G., Rodriguez-Martin, J. E., Díaz-García, L. A., et al. 2022, A&A, 666, A84
Di Matteo, T., Springel, V., & Hernquist, L. 2005, Nature, 433, 604
Dressler, A. 1980, ApJ, 236, 351
Elbaz, D., Daddi, E., Borgne, D. L., et al. 2007, A&A, 468, 33
Erfanianfar, G., Popesso, P., Finoguenov, A., et al. 2016, MNRAS, 455, 2839
Fanidakis, N., et al. 2012, MNRAS, 419, 2797
Fasano, G., Poggianti, B. M., Bettoni, D., et al. 2015, MNRAS, 449, 3927
Ferrarese, L., & Merritt, D. 2000, ApJ, 539, 9
Florez, J., Jogee, S., Sherman, S., et al. 2020, MNRAS, 497, 3273
Hasan, F., Burchett, J. N., Abeyta, A., et al. 2023, ApJ, 950, 114
Hopkins, P. F., Hernquist, L., Cox, T. J., & Keres, D. 2008, ApJS, 175, 356
Inoue, A. K. 2011, MNRAS, 415, 2920
Kauffmann, G., Heckman, T. M., White, D. M. S., et al. 2003, MNRAS, 341, 33
Komatsu, E., Smith, K. M., Dunkley, J., et al. 2011, ApJS, 192, 18
Kormendy, J., & Ho, L. C. 2013, ARA&A, 51, 511
Koutoulidis, L., Mountrichas, G., Georgantopoulos, I., Pouliasis, E., & Plionis, M. 2022, A&A, 658, A35
Laigle, C., McCracken, H. J., Ilbert, O., et al. 2016, ApJS, 224, 24
Lanzuisi, G., Delvecchio, I., Berta, S., et al. 2017, A&A, 602, 13
Leslie, S. K., Schinnerer, E., Liu, D., et al. 2020, ApJ, 899, 58
Lin, L., Jian, H.-Y., Foucaud, S., et al. 2014, ApJ, 782, 33
Loh, J. M. 2008, ApJ, 681, 726
Lutz, D., Mainieri, V., Rafferty, D., et al. 2010, ApJ, 712, 1287
Magorrian, J., Tremaine, S., Richstone, D., et al. 1998, AJ, 115, 2285
Małek, K., Buat, V., Roehlly, Y., et al. 2018, A&A, 620, A50
Marchesi, S., Civano, F., Elvis, M., et al. 2016, ApJ, 817, 34
Masoura, V. A., Mountrichas, G., Georgantopoulos, I., et al. 2018, A&A, 618, 31
Masoura, V. A., Mountrichas, G., Georgantopoulos, I., & Plionis, M. 2021, A&A, 646, A167
McCracken, H. J., Milvang-Jensen, B., Dunlop, J., et al. 2012, A&A, 544, A156
Meenakshi, M., Mukherjee, D., Wagner, A. Y., et al. 2022, MNRAS, 511, 1622
Mountrichas, G., Georgakakis, A., & Georgantopoulos, I. 2019, MNRAS, 483, 1374
Mountrichas, G., Buat, V., Yang, G., et al. 2021, A&A, 653, A74
Mountrichas, G., Buat, V., Yang, G., et al. 2022a, A&A, 663, A130
Mountrichas, G., Buat, V., Yang, G., et al. 2022b, A&A, 667, A145
Mountrichas, G., Masoura, V. A., Xilouris, E. M., et al. 2022c, A&A, 661, A108
Mullaney, J. R., Alexander, D. M., Aird, J., et al. 2015, MNRAS, 453, L83
Nelson, D., Springel, V., Pillepich, A., et al. 2019, Comput. Cosmol. Astrophys., 6, 2
Ni, Q., Brandt, W. N., Yang, G., et al. 2021, MNRAS, 500, 4989
Page, M. J., Symeonidis, M., Vieira, J. D., et al. 2012, Naure, 485, 213
Pandey, B., & Sarkar, S. 2020, MNRAS, 498, 6069
Park, T., Kashyap, V. L., Siemiginowska, A., et al. 2006, ApJ, 652, 610
Pérez-Millán, D., Fritz, J., González-López zlira, R. A., et al. 2023, MNRAS, 521, 1292
Pillepich, A., Springel, V., Nelson, D., et al. 2018, MNRAS, 473, 4077
Pouliasis, E., Mountrichas, G., Georgantopoulos, I., et al. 2022, A&A, 667, A56
Rosario, D. J., Trakhtenbrot, B., Lutz, D., et al. 2013, A&A, 560, A72
Santoro, F., Oonk, J. B. R., Morganti, R., Oosterloo, T. A., & Tadhunter, C. 2016, A&A, 590, A37
Santos, J. S., Altieri, B., Tanaka, M., et al. 2014, MNRAS, 438, 2565
Scoville, N., Aussel, H., Brusa, M., et al. 2007, ApJS, 172, 1
Scoville, N., Arnouts, S., Aussel, H., et al. 2013, ApJS, 206, 3
Sobral, D., Smail, I., Best, P. N., et al. 2013, MNRAS, 428, 1128
Sobral, D., van der Wel, A., Bezanson, R., et al. 2022, ApJ, 926, 117
Song, J., Fang, G., Gu, Y., Lin, Z., & Kong, X. 2023, ApJ, 950, 130
Stalevski, M., Fritz, J., Baes, M., Nakos, T., & Popović, L. Č. 2012, MNRAS, 420, 2756
Stalevski, M., Ricci, C., Ueda, Y., et al. 2016, MNRAS, 458, 2288
Straatman, C. M. S., van der Wel, A., Bezanson, R., et al. 2018, ApJS, 239, 27
Sutherland, W., & Saunders, W. 1992, MNRAS, 259, 413
Taylor, M. B. 2005, in Astronomical Data Analysis Software and Systems XIV, eds. P. Shopbell, M. Britton, & R. Ebert, ASP Conf. Ser., 347, 29
Tremaine, S., Gebhardt, K., Bender, R., et al. 2002, ApJ, 574, 740
van der Wel, A., Noeske, K., Bezanson, R., et al. 2016, ApJS, 223, 29
van der Wel, A., Bezanson, R., D'Eugenio, F., et al. 2021, ApJS, 256, 44
Wu, P.-F., van der Wel, A., Gallazzi, A., et al. 2018, ApJ, 855, 85
Yang, G., Brandt, W. N., Darvish, B., et al. 2018, MNRAS, 480, 1022
Yang, G., Brandt, W. N., Alexander, D. M., et al. 2019, MNRAS, 485, 3721
Yang, G., Boquien, M., Buat, V., et al. 2020, MNRAS, 491, 740
Yang, G., Boquien, M., Brandt, W. N., et al. 2022, ApJ, 927, 192
Zinn, P.-C., Middelberg, E., Norris, R. P., & Dettmar, R.-J. 2013, ApJ, 774, 66
Zubovas, K., Nayakshin, S., King, A., & Wilkinson, M. 2013, MNRAS, 433, 3079